SANDIA REPORT

SAND89—3073 • UC—600
Unlimited Release
Printed January 1990

Hybrid Thin-Slot Algorithm for the Analysis of Narrow Apertures in Finite-Difference Time-Domain Calculations

Douglas J. Riley, C. David Turner

Prepared by
Sandia National Laboratories
Albuquerque, New Mexico 87185 and Livermore, California 94550
for the United States Department of Energy
under Contract DE-AC04-76DP00789

Issued by Sandia National Laboratories, operated for the United States Department of Energy by Sandia Corporation.

Printed in the United States of America. This report has been reproduced directly from the best available copy.

Available to DOE and DOE contractors from
Office of Scientific and Technical Information
PO Box 62
Oak Ridge, TN 37831

Prices available from (615) 576-8401, FTS 626-8401

Available to the public from
National Technical Information Service
US Department of Commerce
5285 Port Royal Rd
Springfield, VA 22161

NTIS price codes
Printed copy: A03
Microfiche copy: A01

SAND89–3073
Unlimited Release
Printed January 1990

Distribution
Category UC–600

Hybrid Thin–Slot Algorithm for the Analysis of Narrow Apertures in Finite–Difference Time–Domain Calculations

Douglas J. Riley and C. David Turner

Electromagnetic Applications Division
Sandia National Laboratories
Albuquerque, NM 87185

ABSTRACT

The modeling of apertures that are narrow with respect to the spatial cell size is a well–known problem for finite–difference time–domain (FDTD) electromagnetic codes. Although the *possibility* of using "half–space" transient integral equations to characterize narrow apertures in FDTD codes has been suggested and studied by others, a solution to the fundamental problem of how the two techniques could be combined so that full coupling to the aperture is accounted for was unknown. A scheme which resolves this problem is presented here. To introduce the technique, only linear apertures that are electrically narrow with regard to both their width and depth are discussed, but extensions to more complex aperture configurations should be possible. The method incorporates an independent "time–marching" solution for the aperture problem into the FDTD code, and therefore, the burden of gridding the aperture by a general–purpose FDTD code is avoided. A feedback scheme is used so that full exterior and interior coupling is included in the aperture solution. This "hybrid thin–slot algorithm" (HTSA) is quite easy to implement, yields high accuracy, and gives rise to a "one–step" FDTD solution.

LIST OF CONTENTS

LIST OF FIGURES

I. INTRODUCTION

General–purpose finite–difference time–domain (FDTD) codes are widely used for modeling the electromagnetic response of systems with low to moderate complexity. The basic discretizing algorithm that these codes generally follow is due to Yee [1]. Although Yee's work appeared in 1966, it has only been within the past decade that FDTD codes have gained widespread popularity within the electromagnetics community as a whole, even though within the EMP community the utility of FDTD had been recognized since the early 1970's [2]. The relatively slow widespread utilization of FDTD is perhaps due to the fact that the development of general–purpose codes required the resolution of many technical difficulties not addressed in Yee's original paper [3], and the computer resources required to run these codes can often be excessive. The latter is especially true when one would like to use FDTD to make calculations that are valid into the microwave frequency region.

As an example of these computer requirements, consider the following. Suppose that one desired to model a hollow rectangular box that is only 20 cm on a side. If one were to use a uniform spatial cell of, say, 1 mm, which would lead to a solution spectrum that is valid up to 20–30 GHz, computer time and/or memory requirements for this seemingly simple problem could easily stress some of the largest supercomputers. Increasing the spatial cell size to 1 cm, for example, reduces the resource requirements to tractable levels, but details that may require a 1–mm spatial cell can no longer be resolved, and the spectrum of the solution will only to accurate to 2–3 GHz (or slightly higher if one is willing to accept less than 10 cells/wavelength).

Nowhere is the resolution problem more important than in the characterization of apertures. If the physical size of the aperture is on the order of, or larger than the spatial cell size, then modeling this aperture is generally not a problem because it can be gridded. However, if the aperture is narrow with respect to

the spatial cell, one must either reduce the cell size for the *entire* problem down to that required to resolve the aperture, or adopt an alternative method to characterize the aperture. As noted above, reducing the cell size is often not a feasible approach, and therefore alternative methods must be investigated.

One of the earliest investigations into this problem was by Gilbert and Holland [4]. Their algorithm, known as the "thin–slot formalism" (TSF), recognizes that the capacitance of the slot varies strongly with width, and therefore knowledge of the slot capacitance (and inductance) enables one to create modified field equations local to the aperture without reducing the overall spatial cell size. An inherent problem with this technique, of course, is the *a priori* description of the electrical parameters of the slot. By assuming that the transverse electric field within the aperture behaves as a constant, which is a reasonable assumption for electrically narrow slots with depth, the Gilbert–Holland algorithm basically simplifies to that described by Taflove, *et al.* [3]. Taflove, *et al.*, applied their algorithm to two–dimensional narrow aperture problems with depth. The results of this TSF compared favorably with results obtained by modeling the slots using two–dimensional moment–method techniques. It is noted that the TSF gives rise to a "one–step" FDTD solution.

An investigation by Turner and Bacon [5] into the accuracy of the TSF for two– and three–dimensional slots in infinitely thin walls demonstrated that the thin–slot formalism tends to increasingly underestimate the aperture electric field as the width of the aperture decreases. An explanation for this was given as follows. When the depth of the wall is taken to be zero there can only be one transverse electric–field sample point through the aperture. The magnitude of this field, of course, increases with decreasing aperture width. Because finite–difference codes give average field values throughout a cell, and the cell of interest for this aperture can be taken to extend from one–half cell in front of the wall to one–half cell behind the

wall, the predicted *average* electric field will be lower than the true field directly in the gap. The discrepancy will increase as the width of the aperture decreases, as observed. This can be an important consideration if one defines conducting walls on electric–field evaluation points. The study by Taflove [3] generally found superior accuracy of the TSF. A possible explanation for this is that slots with *depth* were investigated in that study, and no E–field evaluation points were in the entering or exiting planes of the slot; in other words, averaging the gap E–field was restricted to averages taken *within* the slot. It is noted that a *fully gridded* solution may suffer a similar problem, but because one generally does not grid such narrow apertures the problem has not been observed.

Other techniques to model apertures in FDTD codes generally take advantage of the well–known equivalence principle. A hybrid frequency–domain moment–method/FDTD scheme was proposed by Taflove and Umashankar [6]. Their technique uses the moment method to model the closed exterior region of the scatterer to obtain a "short–circuit" term that is used to drive the interior region, which is modeled by FDTD. The technique gives rise to a four–step solution process. A similar technique by Merewether and Fisher [7] models both the exterior and interior using FDTD, resulting in a two–step process. A benefit of this two–step technique is that when the interior region is solved, one need only "loosely" grid the exterior region which can result in considerable savings in computer resources. Although these multi–step techniques can be of value, they are not suitable for narrow apertures unless one uses the TSF as well, because the aperture must be left open when the interior problem is solved by FDTD. However, by successively applying the equivalence principle, Demarest [8] was able to perform an FDTD analysis of a narrow aperture coupling into a cavity. This approach gave rise to a four–step solution process. Another technique to model narrow apertures is the use of "sub–gridding" local to the aperture [9]. This approach has been found to be difficult to code, and requires care in its implementation

to avoid numerical reflections off the interface between the various meshes.

Although the *possibility* of using "half–space" transient integral equations to characterize narrow apertures in FDTD codes has been suggested and studied by others, a solution to the fundamental problem of how the two techniques could be combined so that full coupling is accounted for was unknown. A scheme which resolves this problem is presented here. To introduce the technique, linear apertures that are electrically narrow with regard to both their width and depth are discussed. The dual of the well–known Pocklington equation is solved using an explicit (time–marching) finite–difference solution. The solution is used as a magnetic current element in appropriate curl–E equations in the FDTD code. The inclusion of depth is possible by using an equivalent antenna radius recently derived for deep slots [10].

One may argue that solving the Pocklington equation is appropriate provided one will be satisfied with an aperture distribution associated with radiation into an empty half space. However, by judiciously using the FDTD code for field predictions local to the aperture, it is possible to create a feedback technique that includes all interior and exterior coupling to the aperture. This is useful because it permits one to incorporate half–space integral–equation formulations into FDTD codes, without requiring specific Green's functions to be known. Thus, extension of the basic hybrid technique to more complex narrow apertures should indeed be possible.

To implement the hybrid thin–slot algorithm (HTSA), one only needs to: (1) keep track of the internal and external total H–fields local to the desired aperture position, and (2) append a magnetic current element to the appropriate H–field equations at each time step. This hybrid scheme gives rise to a one–step solution process. Advantages of this approach include: (1) A very accurate description for the slot physics because the slot is characterized by an integral–equation formulation; (2) The ability to accommodate, to some extent, tortuous depth paths simply by changing the depth parameter in the slot algorithm [10]; and (3) It is not susceptible to the

"averaging problem" associated with the TSF that can result in the underestimation of aperture fields noted above. A disadvantage of the scheme presented here is that one is limited to linear apertures oriented along principal axes; however, as noted above, because the method is based on incorporating transient half–space integral–equation solutions, extensions to more complex aperture configurations should be possible. Butler and Reed [11] have pursued using explicit finite–difference techniques to solve the transient equations associated with multiple narrow apertures in infinitely thin conducting planes. Solutions of this type are candidates for the hybrid algorithm.

The organization of the paper is as follows. In section II, an explicit, or time–marching finite–difference scheme for the slot problem is presented, and the feedback technique to include interior and exterior coupling to the aperture is described. In section III, the HTSA is used to analyze coupling into rectangular cavities that are loaded with wires and boxes. Comparisons are made with results obtained by a fully gridded solution (where feasible) and results obtained by using the TSF. Concluding remarks are made in section IV.

II. ANALYSIS

The geometry of a linear slot of length L and width w in an infinite plane is shown in Figure 1. Observe that the aperture is assumed to lie along the x axis. For sources on both sides of the plane, the well–known transient equation that describes the dominant coupling for this problem is given by

$$\mu_0 \frac{\partial}{\partial t} H_x^{sc1} + 2\left(\frac{\partial^2}{\partial x^2} - \frac{1}{c^2}\frac{\partial^2}{\partial t^2}\right) \int_{-L/2}^{L/2} dx' \frac{K_x(x';t-|x-x'|/c)}{2\pi\sqrt{a^2+(x-x')^2}} = \mu_0 \frac{\partial}{\partial t} H_x^{sc2}, (-L/2 \leq x \leq L/2) \tag{1}$$

where

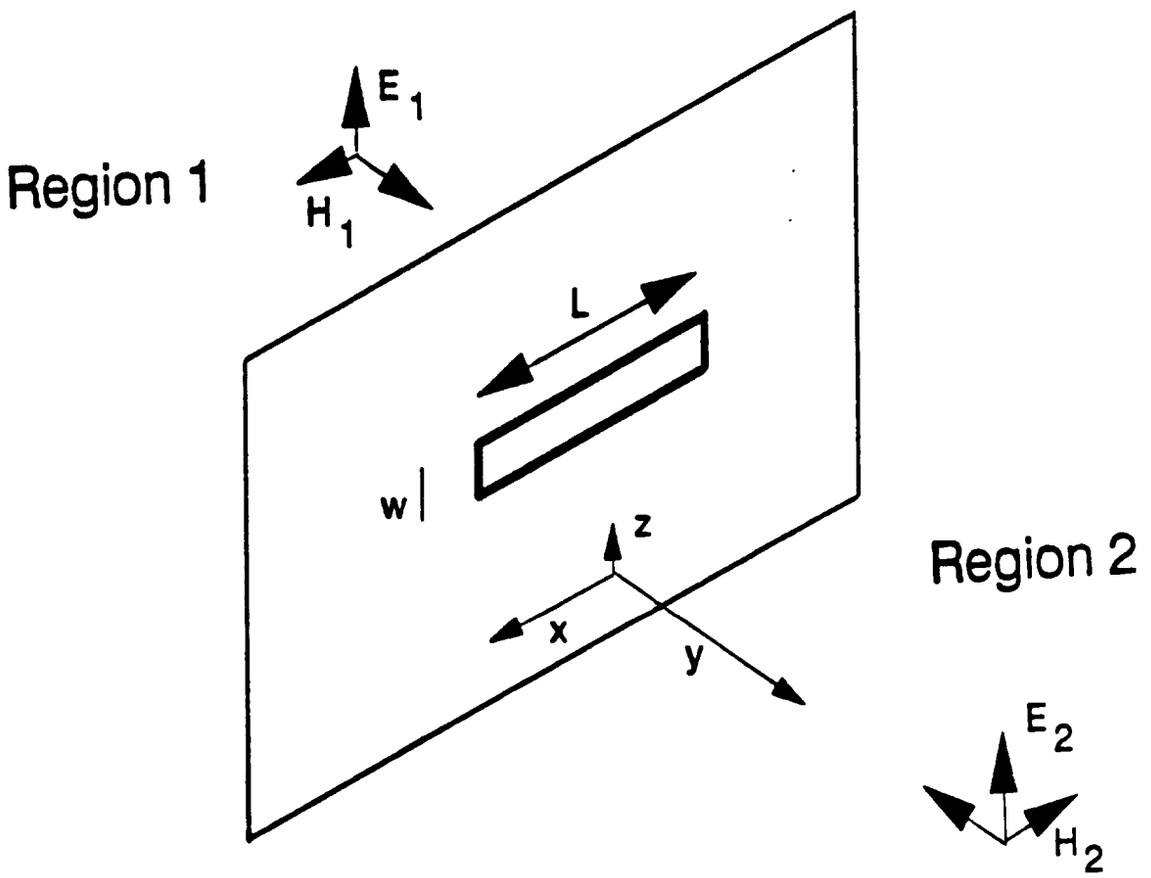

Figure 1: Geometry for a three–dimensional slot in an infinitely thin conducting wall.

c	denotes the speed of light in vacuum,
μ_0	denotes the permeability of free space,
H_x^{sc1}	denotes the short–circuit field in front of the slot (region 1),
H_x^{sc2}	denotes the short–circuit field behind the slot (region 2),
K_x	denotes the total magnetic current,
t	denotes the time dependence,
a	denotes the equivalent antenna radius for the slot.

Eq. (1) represents the dual equation to the Pocklington equation of antenna theory.

The total magnetic current in Eq. (1) and the magnetic current *density*, M_x, are related by

$$K_x(x,t) = \int_{-w/2}^{w/2} dz\, M_x(z,x,t).$$

Since $\hat{y}$ is assumed to be directed into region 2, M_x in region 1 is related to the transverse electric field in the gap, E_{gap}, by $\hat{x}\, M_x = \hat{y} \times (\hat{z}\, E_{gap})$. In region 2, the magnetic current density changes sign. Observe that the average electric field across the gap can be written as K_x/w.

For slots with zero depth, Eq. (1) has been widely used with $a = w/4$. For slots with depth d, the equivalent radius $a = (w/4)\exp(-\pi\, d/2\, w)$ is used [10]. The validity of (1) with this radius requires the following: (1) $L/w >> 1$, and (2) w and d are both electrically small. Observe that slot depth resonances are ignored by this formulation and that E_{gap} is assumed to be uniform throughout the gap depth. It is noted that many practical narrow apertures are much longer than either their width or depth; thus, ignoring depth resonances will only be a problem if the illumination has significant very high frequency content (typically several gigahertz, and such high frequencies may not even be resolvable in a general–purpose FDTD code because of frequency limitations imposed by the largest cell size).

To solve equation (1) using a finite–difference scheme, the following procedure is performed. First, K_x is expanded as

$$K_x(x',\tau) = \sum_{n'=1}^{N} \sum_{p'=-\infty}^{\infty} K_{n',p'}\, P_{\Delta t}(\tau - p'\Delta t)\, P_{\Delta}(x' - n'\Delta)\,,$$

where Δ defines the spatial step along the axis of the slot equal to $L/(N+1)$, and Δt denotes the time step. It is noted that Δ will *not*, in general, be equal to the spatial step used in the main FDTD code. Further comments on this will be made below. $P_{\Delta t}$ and P_{Δ} denote standard unit pulse functions with widths Δt and Δ, respectively. $K_{n',p'}$ denotes the unknown coefficients at spatial position $n'\Delta$ and time $p'\Delta t$.

With this expansion, the integral in (1) can be written approximately as

$$\int_{-L/2}^{L/2} dx' \left. \frac{K_x(x';t-|x-x'|/c)}{2\pi\sqrt{a^2+(x-x')^2}} \right|_{\substack{x=n\Delta \\ t=p\Delta t}} \cong$$

$$\sum_{n'=1}^{N} \sum_{p'=-\infty}^{\infty} K_{n',p'}\, P_{\Delta t}((p-p')c\Delta t - |n-n'|\Delta) \int_{(|n-n'|-\frac{1}{2})\Delta}^{(|n-n'|+\frac{1}{2})\Delta} d\eta\, \frac{1}{2\pi\sqrt{a^2+\eta^2}}\,.$$

Extracting the time pulse from the integral is only valid for very thin, linear structures. By defining $p' = p - |n-n'|$, which assumes $c\Delta t = \Delta$ for the slot–solution algorithm, and using central differences for all differential operators appearing in (1), the following explicit difference scheme may be obtained for the coefficients $K_{n',p'}$:

$$K_{n,p} = \frac{1}{2}\frac{\mu_o}{\Delta t}\frac{\Delta^2}{G_o}\left[\left(H^{sc1}_{x_{n,p-1}} - H^{sc1}_{x_{n,p-2}}\right) - \left(H^{sc2}_{x_{n,p-1}} - H^{sc2}_{x_{n,p-2}}\right)\right] +$$

$$+ K_{n+1,p-1} + K_{n-1,p-1} - K_{n,p-2} +$$

$$\frac{1}{G_o}\sum_{\substack{n'=0 \\ n\neq n'}}^{N+1} G_{|n-n'|}\left[K_{n'+1,p-1-|n-n'|} + K_{n'-1,p-1-|n-n'|} - K_{n',p-|n-n'|} - K_{n',p-2-|n-n'|}\right], \quad \begin{bmatrix} n=1,2,3,\ldots,N \\ p=1,2,3,\ldots\ldots \end{bmatrix}, \tag{2}$$

where

$$G_\alpha = \frac{1}{2\pi}\ln\left[\frac{(\alpha+1/2)\Delta + \left[(\alpha+1/2)^2\Delta^2 + a^2\right]}{(\alpha-1/2)\Delta + \left[(\alpha-1/2)^2\Delta^2 + a^2\right]}\right].$$

End conditions require that $K_{0,\xi}$, $K_{-1,\xi}$, $K_{N+1,\xi}$, and $K_{N+2,\xi}$ are defined to be zero for every ξ. In addition, $K_{\nu,\xi}$ is defined to be zero for every ν with $\xi \leq 0$. By time–marching (2), the slot magnetic current is obtained. An average value for the electric field across the aperture is obtained by forming $K_{n,p}/w$, n=1,2,..N; p=1,2,....

Several comments are in order about the spatial step and time step used in the slot solution and their relation to the values used in the main FDTD code. It is convenient to define Δt used in the slot algorithm to be identical to that used in the main FDTD code. To define the spatial step, it is necessary to consider the Courant stability criterion required by each code. Three–dimensional FDTD codes based on the Yee algorithm typically choose a uniform spatial step to be $\Delta_x/2 = \Delta_y/2 = \Delta_z/2 = c\Delta t$. This choice amply satisfies the maximum permitted spatial step required for stability given by $\Delta_x=\Delta_y=\Delta_z= c\Delta t\cdot\sqrt{3}$ [12]. Using the same Δt in the slot algorithm implies that $\Delta = \Delta_x/2$. Thus the spatial step in the slot algorithm is taken to be half that used in the FDTD code, which in turn specifies N. This choice for Δ may be taken because the slot algorithm involves a one–dimensional finite–difference solution,

and therefore a *possible* Courant stability criterion is $c\Delta t \leq \Delta$ for this case (for a discussion on establishing stability criteria for transient integro–differential equation formulations, see refs. [13,14]). As formulated above, the time–marching scheme for the magnetic current takes advantage of the choice $c\Delta t = \Delta$.

Formally, the above solution for the average gap electric field is valid for empty half–spaces existing to the left and right of the plane of the aperture. Different illuminating sources, which generate the short–circuit fields, may exist in regions 1 and 2. Exploiting this fact is what enables the solution to be generalized to arbitrary structures existing to the left and right of the aperture.

Suppose that an object exists behind the aperture. At a given time step the total H–field very close to the aperture consists of two parts: 1) A "half–space" outgoing wave generated at the present time step; and 2) A scattered wave due to aperture fields radiated at earlier times. The outgoing wave at a position $y=y_0$ from the slot is determined from the (half–space) expression

$$\mu_0 \frac{\partial}{\partial t} H_x^{1,2} = \pm \left(\frac{\partial^2}{\partial x^2} - \frac{1}{c^2}\frac{\partial^2}{\partial t^2}\right) \int_{-L/2}^{L/2} dx' \, \frac{K_x(x';t-|x-x'|/c)}{2\pi\sqrt{y_0^2 + (x-x')^2}} \, , (-L/2 \leq x \leq L/2).$$

In time–marching form, the H–field at time–step p–1, n=1,2,...N, can be written as

$$H^{1,2}_{x_{n,p-1}} = H^{1,2}_{x_{n,p-2}} \pm$$

$$\frac{\Delta t}{\mu_0 \Delta^2} \sum_{n'=0}^{N+1} \hat{G}_{|n-n'|} \left[K_{n'+1,p-2-|n-n'|} + K_{n'-1,p-2-|n-n'|} - K_{n',p-1-|n-n'|} - K_{n',p-3-|n-n'|} \right], \quad (3)$$

where,

$$\hat{G}_{\alpha} = \frac{1}{2\pi} \ln \left[\frac{(\alpha+1/2)\Delta + [(\alpha+1/2)^2\Delta^2 + y_0^2]}{(\alpha-1/2)\Delta + [(\alpha-1/2)^2\Delta^2 + y_0^2]} \right].$$

In (3), the "plus" sign is used for region 1 and the "minus" sign is used for region 2.

To obtain the scattered–wave contribution, it is necessary to examine the H–fields used in the main FDTD code that are local to the desired aperture position. Figure 2 depicts the geometry of a thick wall that is defined by electric–field evaluation points in the FDTD mesh. All field quantities generated within the main FDTD code will be denoted by a superscript "FDTD." Observe that the slot does not exist as far as the basic FDTD mesh is concerned; a magnetic current element is used to represent the slot. Also note that the FDTD mesh places H–field evaluation points at positions $y=y_0$ from the wall. Because the aperture is assumed to lie along the x axis, the equation that is modified by the magnetic current element is only the H_x equation in the main FDTD code. The typical modified FDTD equation is (FDTD spatial subscripts omitted)

$$H_{x_p}^{FDTD} = H_{x_{p-1}}^{FDTD} - \frac{\Delta t}{\mu_0} (\nabla \times \bar{E}_{p-1}^{FDTD})_x \pm \left(\frac{\Delta t}{\mu_0} \frac{1}{\Delta_x}\right) \left(\frac{w}{\Delta_x}\right) \left(\frac{1}{w} K_{n,p}\right), \qquad (4)$$

where, in this equation, the "plus" sign is for region 2 and the "minus" sign is for region 1. The terms to the right of the "±" sign define the appropriate magnetic–current element generated by the slot algorithm. The reason the (w/Δ_x) term appears is because the gap electric field must be defined as an average over the entire wall region contained within the FDTD cells local to the aperture; a similar scaling occurred with the TSF [3]. Observe that the modified H–field equation only applies within the cells where the aperture is to exist, both in region 1 and region 2 with the appropriate sign chosen for each region. With (4), all terms required to implement the hybrid thin–slot algorithm are defined.

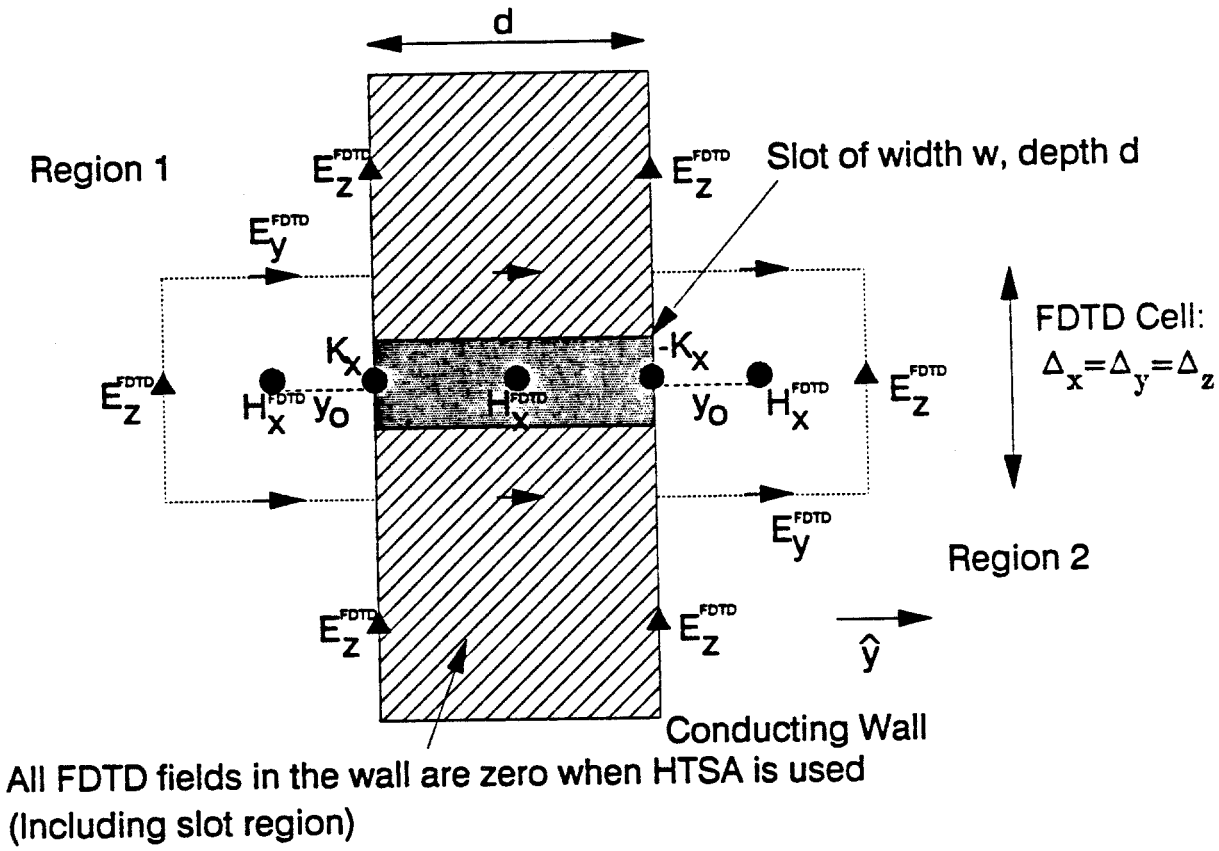

Figure 2: FDTD mesh local to the desired aperture position. All slot information is contained within K_x.

The Hybrid Thin–Slot Algorithm (HTSA)

A self–consistent feedback algorithm can now be established. Let the present time step in the main FDTD code be p. Before the H–fields are advanced (to time–step p) in the FDTD code, a call is made to the HTSA subroutine passing $H^{FDTD}_{x_{p-1}}$ local to the slot, both in region 1 and region 2. The first calculation in the HTSA routine is to determine $H^{1,2}_{x_{n,p-1}}$, which represent the H–fields local to the slot based on "half–space" radiation (cf. Eq. 3). Once the half–space H–fields are found, the short–circuit drive terms are calculated by forming, for region 1,

$$H^{scl}_{x_{n,p-1}} = H^{FDTD}_{x_{p-1}} - H^{1}_{x_{n,p-1}}, \tag{5}$$

with region 2 being similar. Recall that there are twice as many spatial sample points used by the HTSA than in the main FDTD code due to the different spatial step used by each algorithm. For the positions where H^{FDTD}_{x} is not defined, an average value for H^{scl}_{x} can be taken. Figure 3 shows the relationship between H_x evaluation points for the two algorithms.

The operation defined by (5) generates the desired aperture short–circuit excitation term due to reradiation that was induced by previous magnetic–current elements. Once the short–circuit fields are determined, the magnetic current at time–step p can be found from Eq. 2. Return is then made to the main FDTD code, the H–fields are advanced, and the magnetic–current element is included in the appropriate curl–E equation as in (4). In this way, full coupling to the aperture is accomplished. Each time step proceeds similarly. Note that by augmenting the FDTD equations *outside* the H–Advance subroutine, no "vectorizing" loops are disturbed.

One may argue that by forming the field subtraction given by (5), numerical noise is introduced into the FDTD code. This has not been found to be a problem,

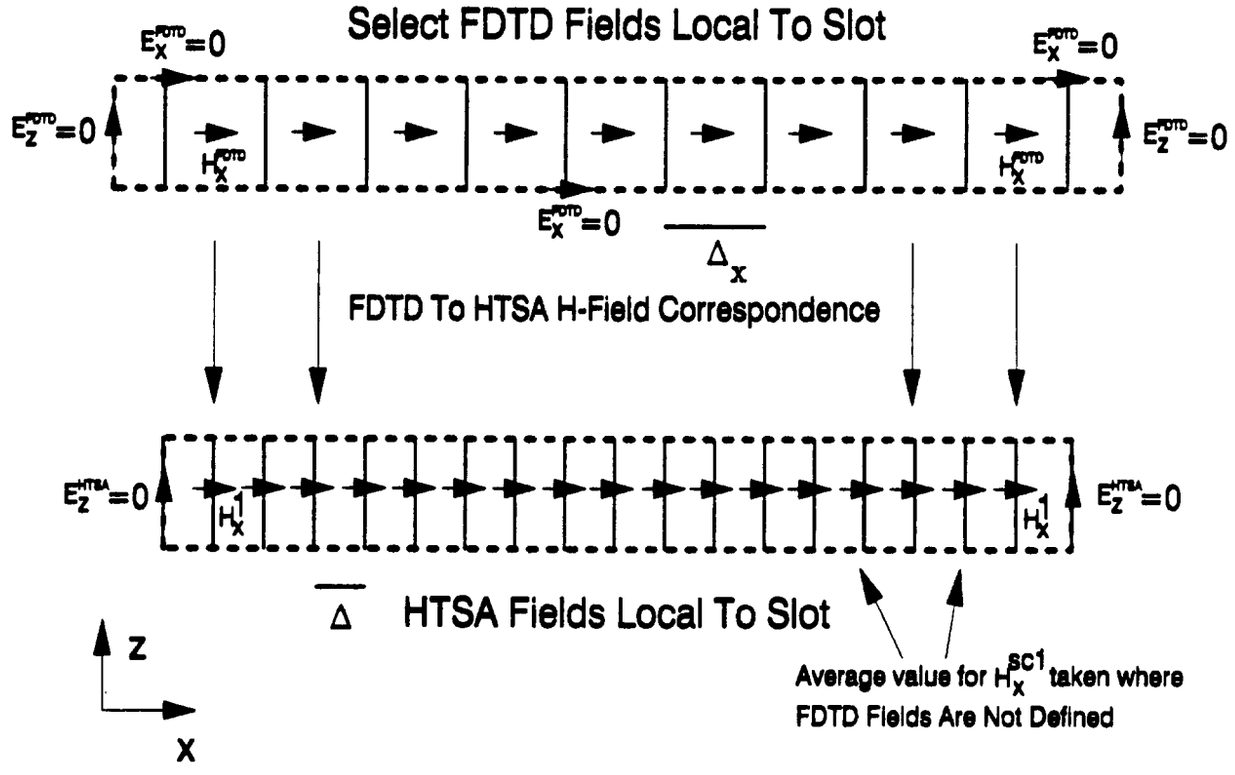

Figure 3: FDTD and HTSA meshes local to the slot showing H–field correspondence as well as differences in slot lengths that result from each mesh.

perhaps because the source terms used to generate the FDTD solution and the half–space solution are of essentially the same form.

III. NUMERICAL RESULTS AND DISCUSSION

For example problems, the geometries shown in Figures 4 and 5 were examined. The spatial cell size used for both problems was 1 cm. The walls of the principal box have a thickness of 1 cm. All structures were made to be perfectly conducting. The interior wire was 6 cm from the inside of the rear wall and 9 cm from the inside of the side walls. The wire was loaded with 50 ohms at each of its ends, and the loads attached to the upper and lower walls of the cavity. The depth of the slot was 1 cm.

The length of the slot used in the HTSA solution was 9 cm. The length of the slot for the gridded solutions, however, was somewhat longer than 9 cm. This is a consequence of the manner in which the FDTD mesh models an aperture. In particular, one can define where tangential electric fields are zero, but due to the sparseness and offset of the Yee mesh, one could consider these points to be *inside a wall* as opposed to defining a boundary condition. Thus, *precisely* where the slot begins and ends is difficult to define when the FDTD mesh is used to grid it. The HTSA does not suffer as seriously from this problem. These comments are visualized in Figure 3.

In Figures 6a and 6b is shown the aperture field for the geometry of Figure 4 with a 1–cm wide slot. In Figure 6a, the feedback scheme discussed above *was not used*; thus, the aperture field used to excite the cavity was as if the aperture was radiating into an empty half space. Comparison is made with results obtained from a full gridded solution. Note that the two solutions agree quite well for the first couple of nanoseconds which is to be expected because it takes some time for the wavefront to "sense" objects behind the aperture. However, in later times the agreement is poor due

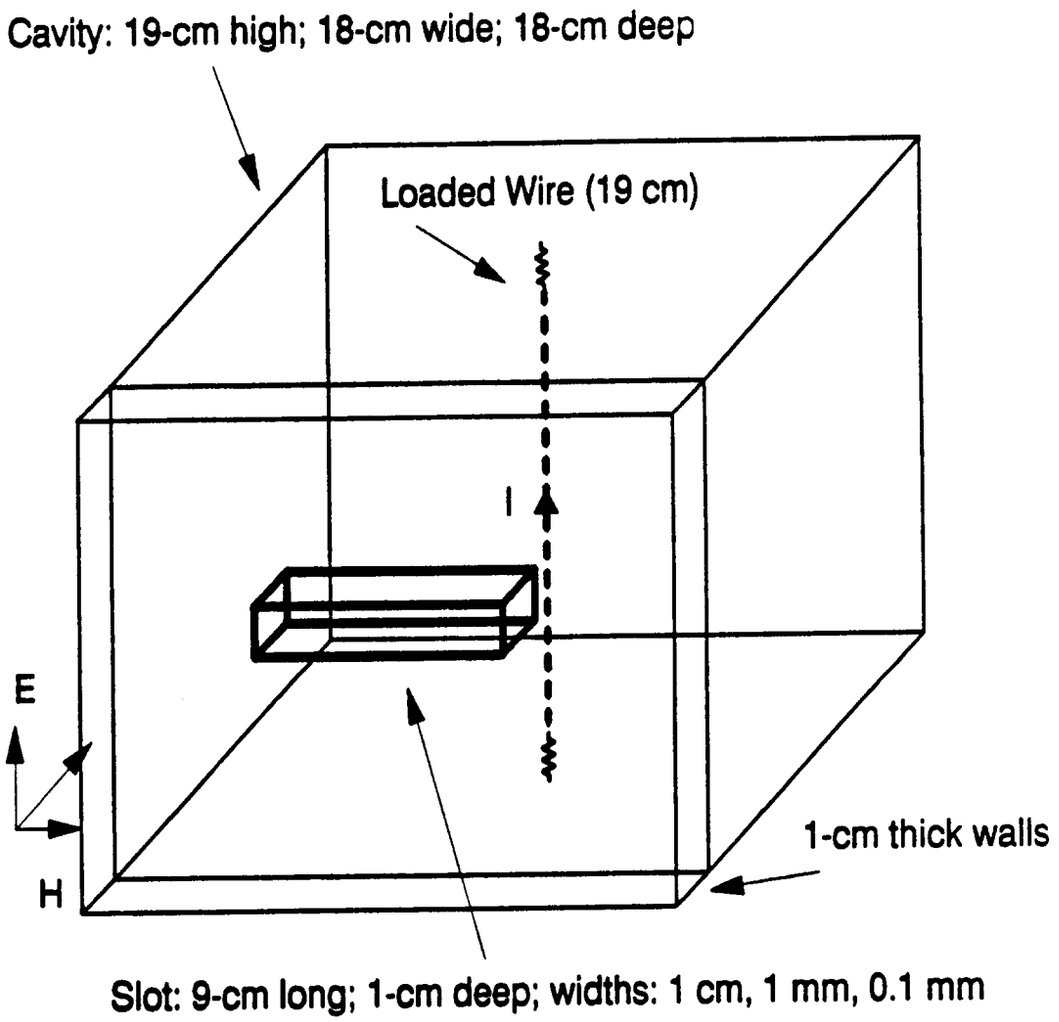

Figure 4: Geometry for test problem 1. All walls are 1–cm thick. The slot is centrally located on the front face.

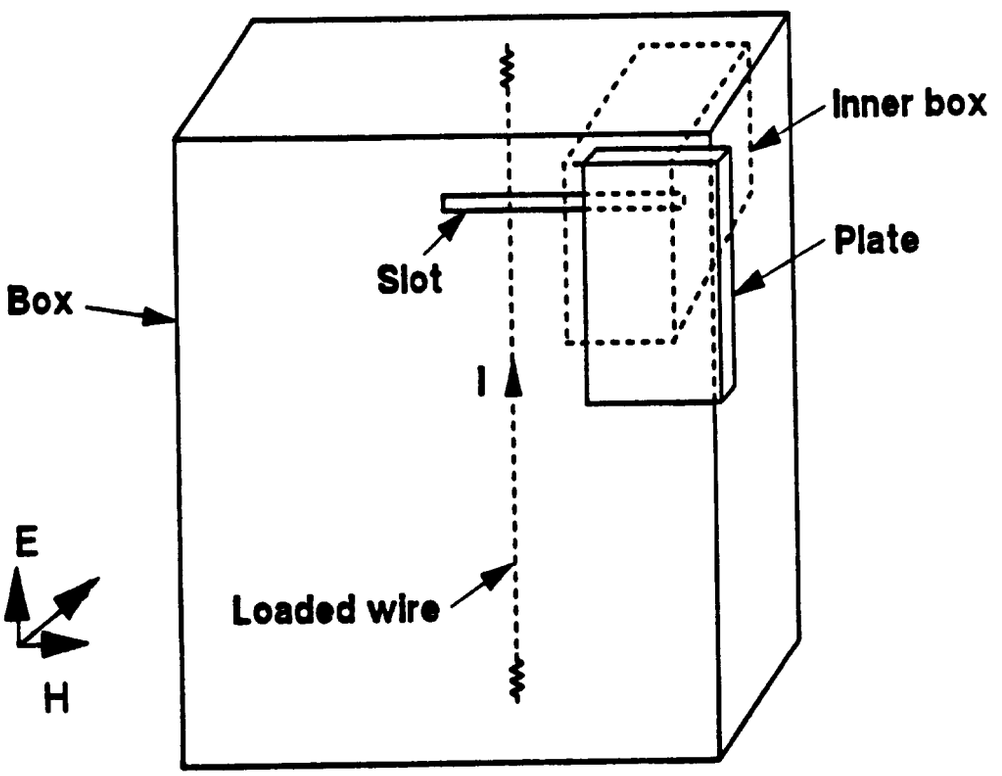

Figure 5: Geometry for test problem 2. This problem is similar to test problem 1, with the following exceptions: (1) The slot is moved to a corner, (2) An internal box is placed 4–cm behind the aperture, and (3) A plate is placed in front of the aperture.

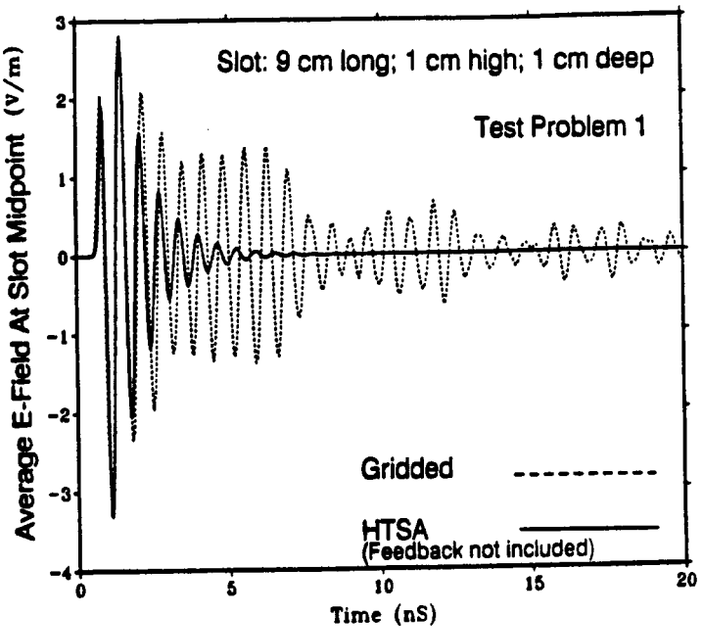

Figure 6a

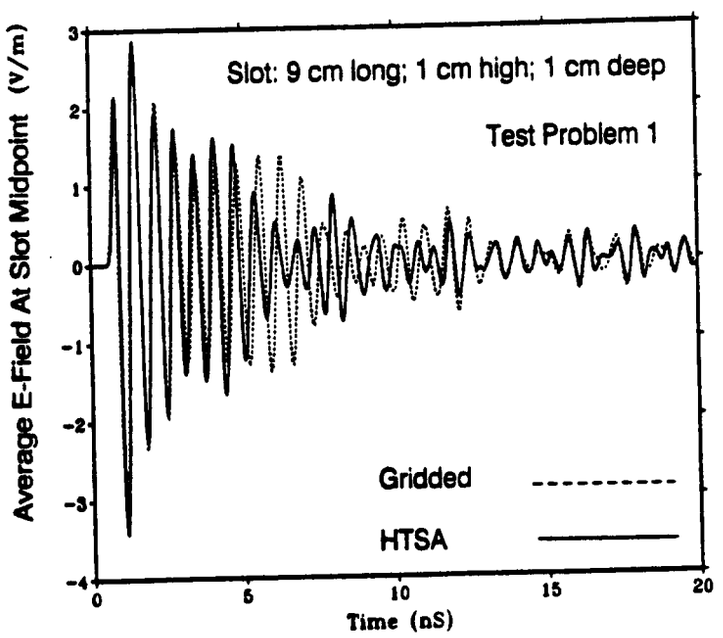

Figure 6b

Figure 6: Gap electric field based on gridding the entire problem, and using the HTSA. (a) Feedback not included with HTSA, (b) Feedback included.

to the cavity redirecting energy back into the aperture, which is ignored when feedback is not included in the HTSA solution. In Figure 6b, the feedback scheme is included and the agreement is seen to be much better for all time. The slight differences in period and modulation are due to the slight differences in slot lengths used in the two solutions, as discussed above. The slot length differences become clear in Figure 7a, which shows the magnitude of the current spectrum at the midpoint of the loaded wire. The first peak corresponds to a cavity resonance, whereas the second peak is the first slot resonance. The gridded result shows a slightly lower resonant frequency corresponding to a slot length slightly longer than the 9–cm length used in the HTSA solution. It is noted that the difference between the frequencies corresponding to the first cavity resonance and the first slot resonance gives rise to the observed modulation on the transient waveforms. The higher–order resonances are due to the cavity and the wire. The null at about 3 GHz is due to the wire response. The transient current response at the wire's midpoint is shown in Figure 7b.

Figures 8–11 show similar results for aperture widths of 1 mm and 0.1 mm. Since these apertures are too narrow to fully grid, comparison is made with results obtained from the TSF. The differences in period and modulation are again due to the slightly different slot lengths used in each approach. The length differences are clear when the current spectrums are viewed. The results obtained from the TSF are believed to be low for the reasons discussed in the introduction. It is noted that wall losses were not a factor in the two solutions, because the walls were forced to be perfectly conducting (a condition which gives rise to a slot Q larger than the cavity Q). If wall losses were included, the slot Q will be lower [15].

Results for the aperture field and wire current for the geometry of Figure 5 are shown in Figures 12 and 13, respectively. Only the 1–cm wide slot was examined because of the superior gridded solution which can be used for comparison. This geometry fully tests the feedback scheme of the HTSA because the slot was placed in

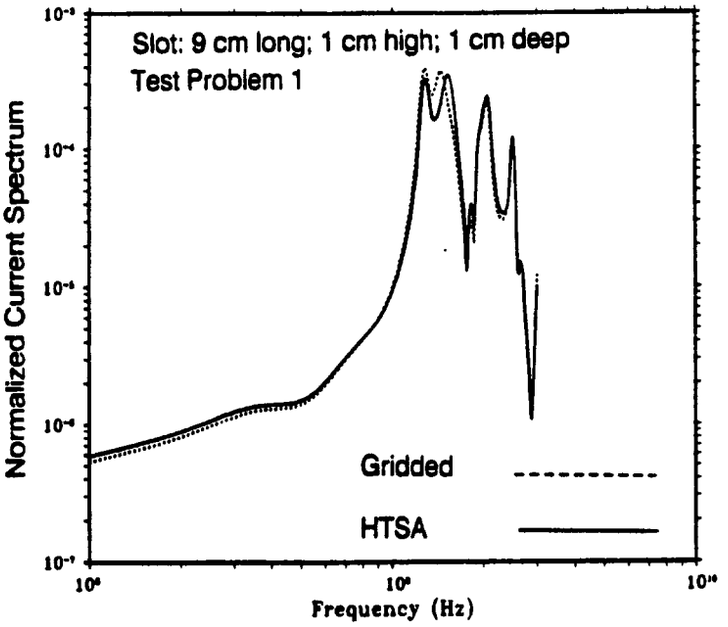

Figure 7a

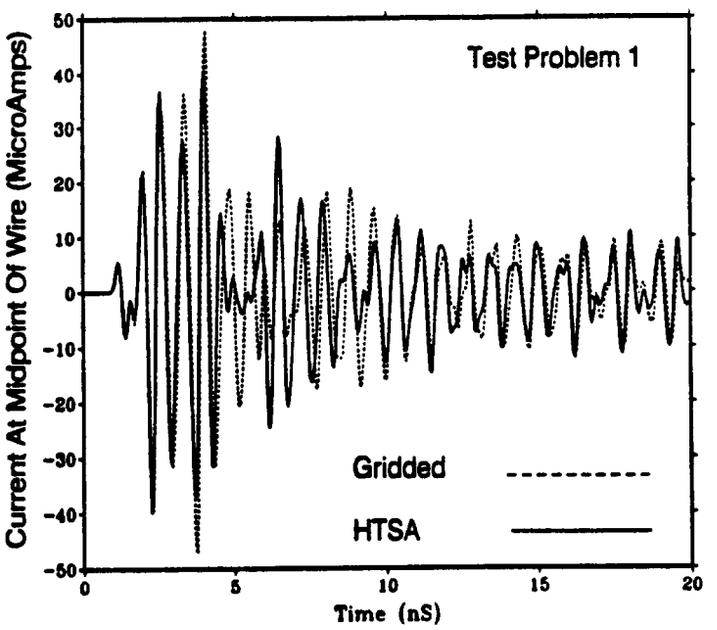

Figure 7b

Figure 7: Current induced at the midpoint of the internal wire. Feedback included with the HTSA solution. 1–cm-wide slot. (a) Spectrum, (b) Transient response.

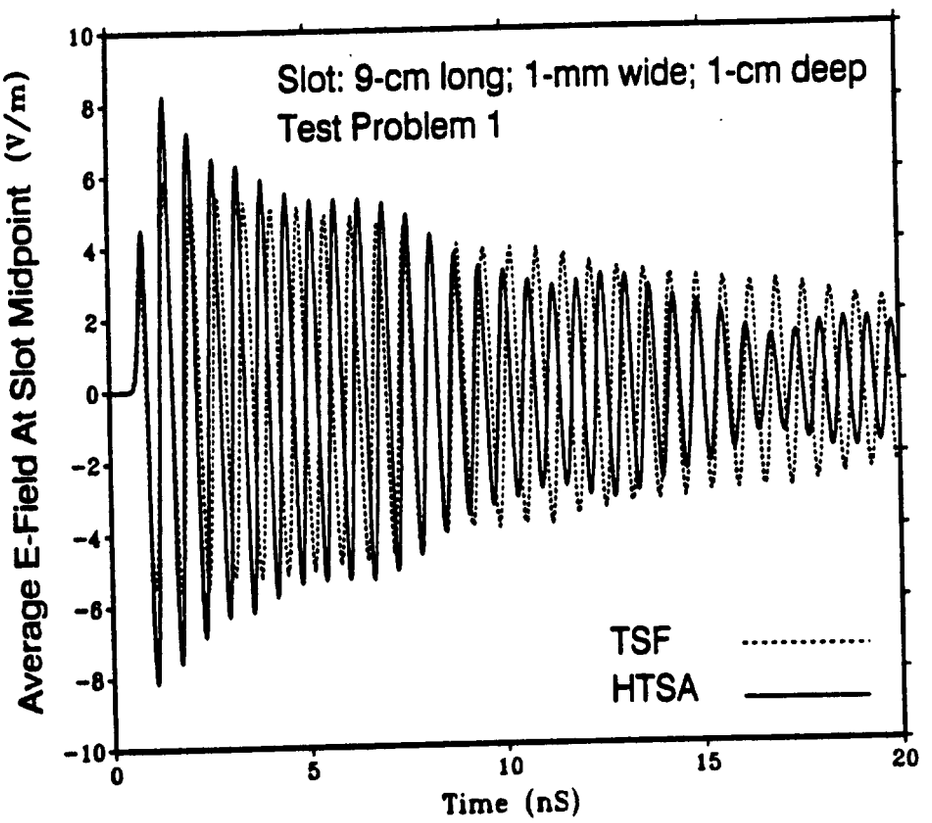

Figure 8: Gap electric field for a 1–mm wide slot. Feedback included in HTSA solution. Comparison made with gridding the aperture using the TSF.

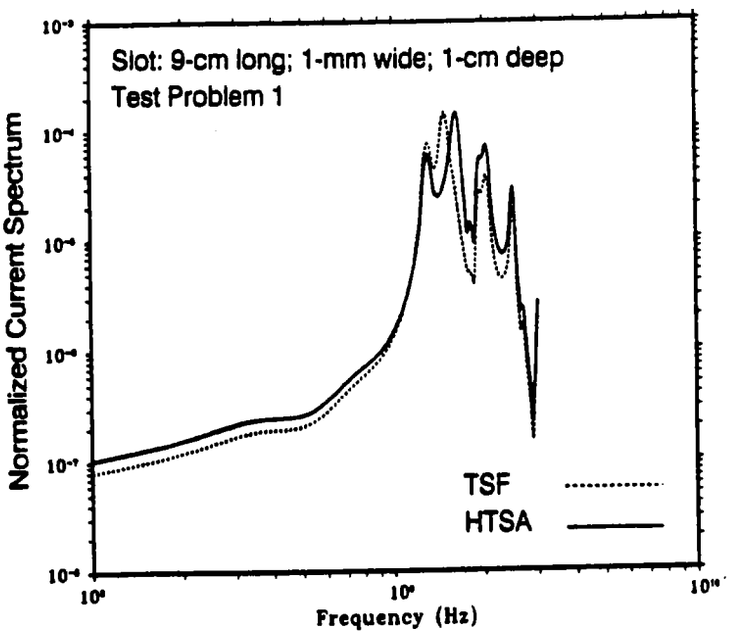

Figure 9a

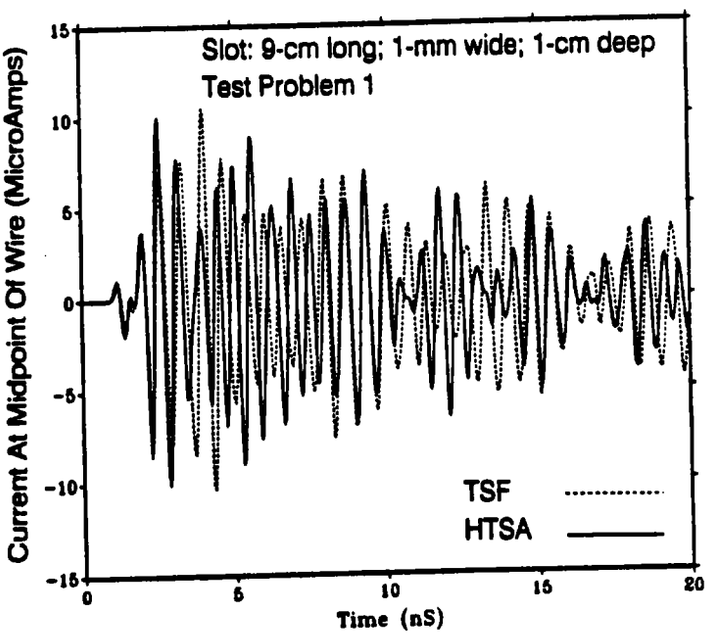

Figure 9b

Figure 9: Current induced at the midpoint of the internal wire. Feedback included with the HTSA solution. 1–mm-wide slot. Comparison made with the TSF. (a) Spectrum, (b) Transient response.

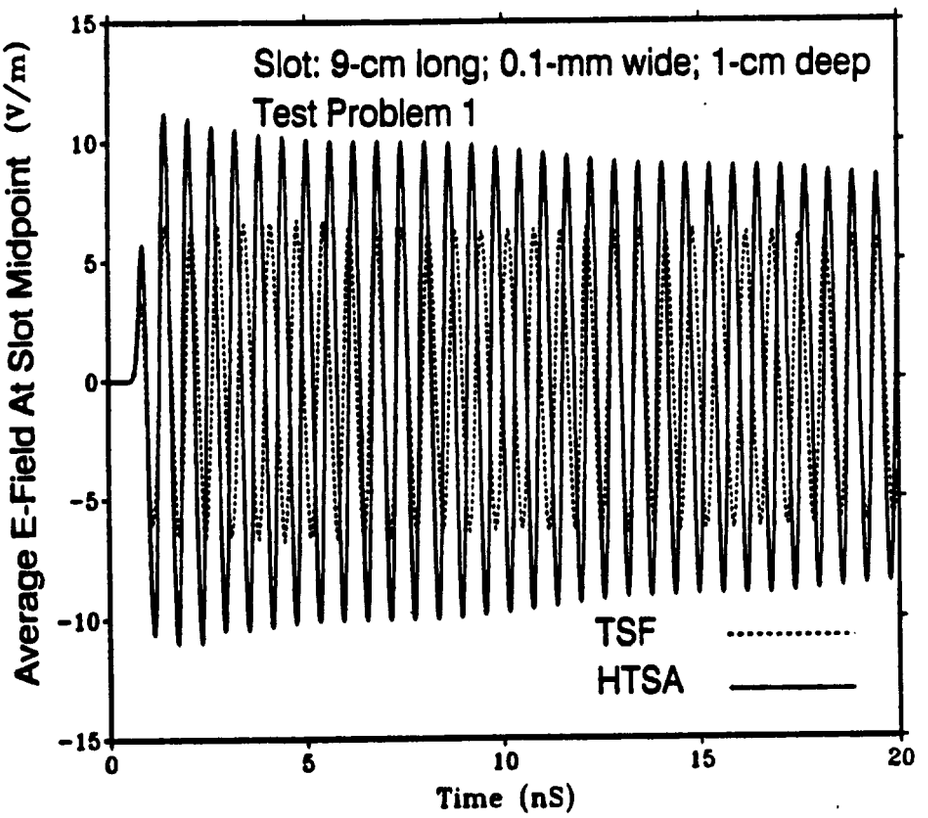

Figure 10: Gap electric field for a 0.1–mm-wide slot. Feedback included in HTSA solution. Comparison made with gridding the aperture using the TSF.

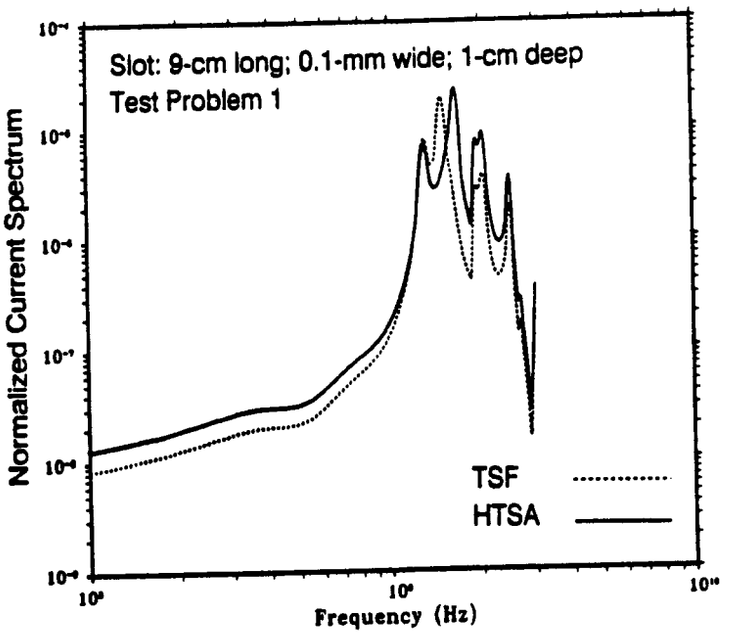

Figure 11a

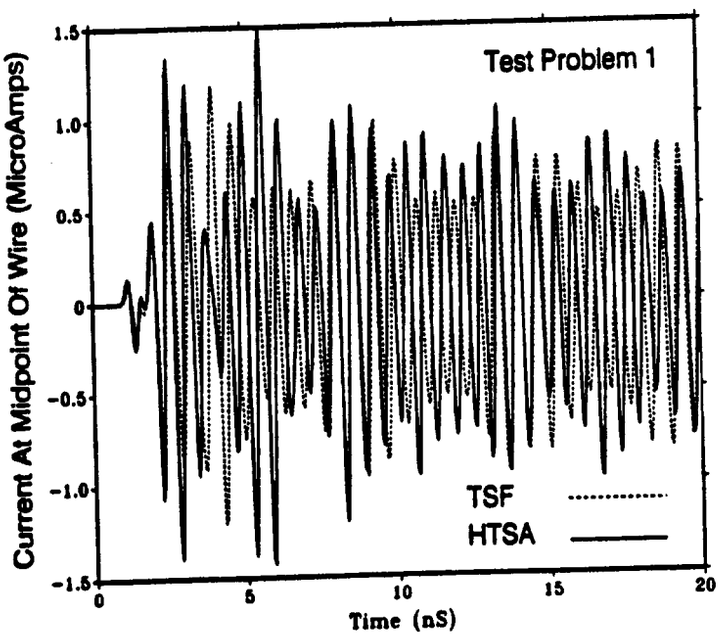

Figure 11b

Figure 11: Current induced at the midpoint of the internal wire. Feedback included with the HTSA solution. 0.1–mm-wide slot. Comparison made with the TSF. (a) Spectrum, (b) Transient response.

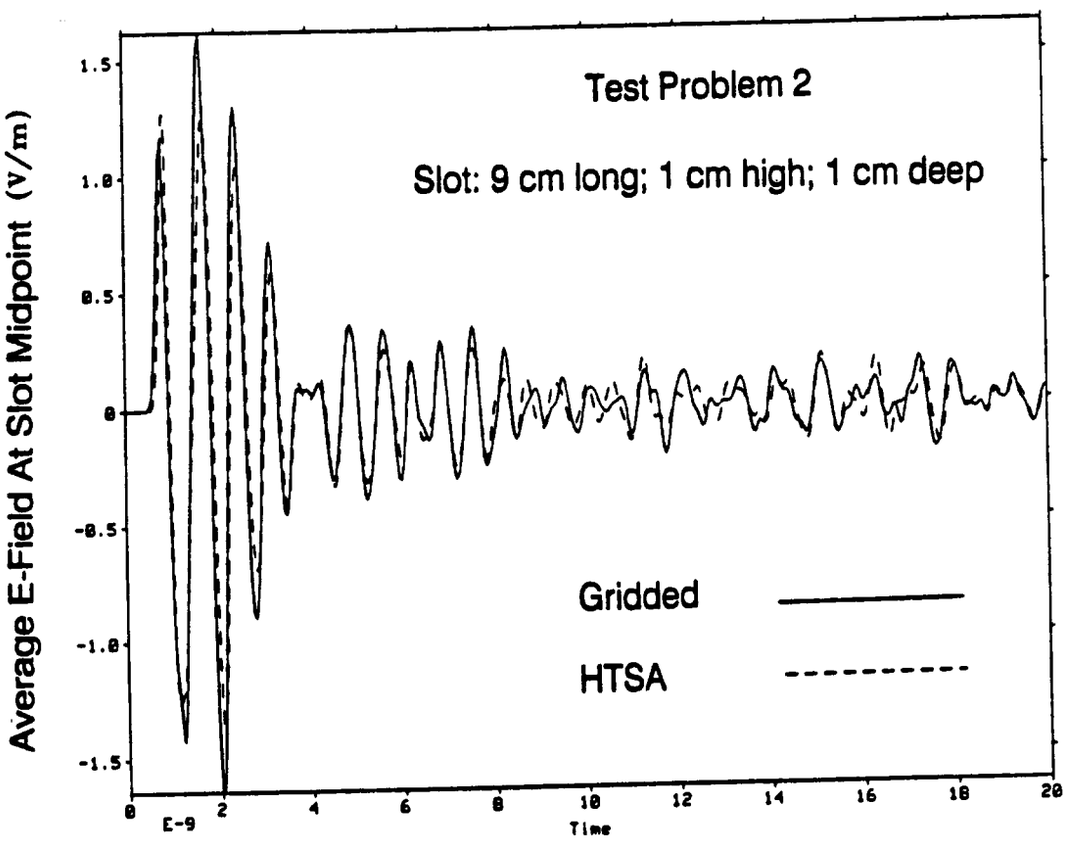

Figure 12: Gap electric field for the 1–cm-wide slot for test problem 2. Feedback included in HTSA solution. Comparison made with a full gridded solution of the problem.

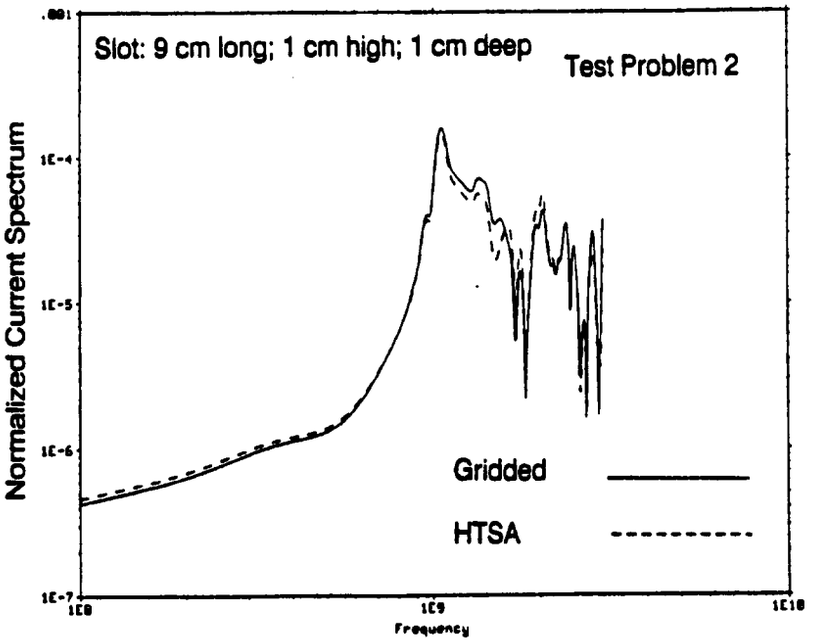

Figure 13a

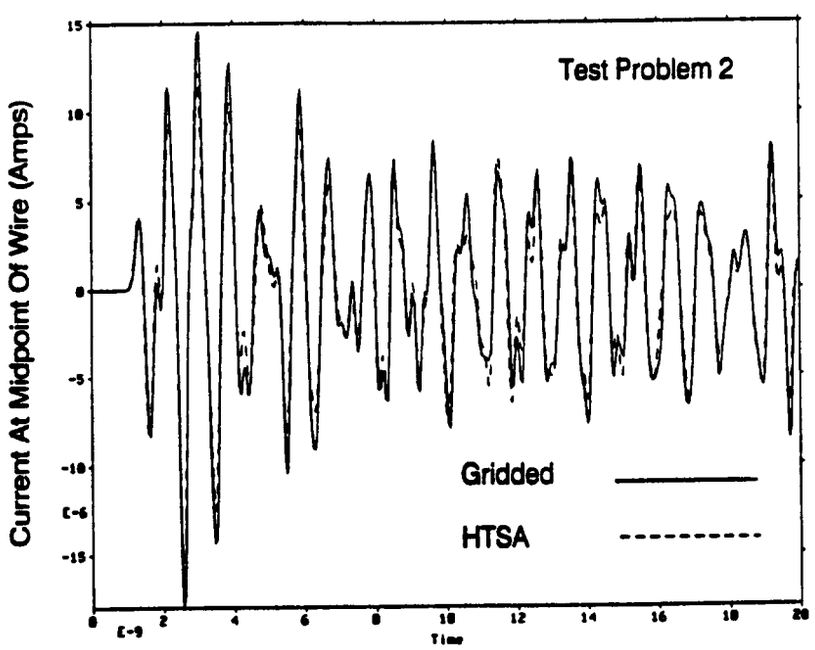

Figure 13b

Figure 13: Current induced at the midpoint of the internal wire for test problem 2. Feedback included with the HTSA solution. 1–cm-wide slot. (a) Spectrum, (b) Transient response.

the corner of the box and additional large obstacles were placed in close proximity both in front of and behind the slot. The agreement is seen to be excellent. The reason these results appear in better agreement than those of test problem 1 is because the significance of the slot resonance has been deemphasized by the obstacles, and therefore the slot length differences are not as important. It is again noted that as far as the FDTD mesh used to model this geometry is concerned when HTSA was used, the slot did not exist, i.e., the cavity was completely closed for this case.

IV. CONCLUDING REMARKS

A new technique for modeling narrow apertures in FDTD codes was proposed in this paper. This technique incorporates an independent time–marching solution for the aperture problem into the FDTD code. A feedback scheme was used so that "half–space" integral–equation formulations can be used to characterize the physics of the aperture. The feedback technique takes advantage of the fact that the FDTD solution for fields local to the aperture are total fields, and therefore the scattered field due to reradiation by obstacles near the aperture can be extracted for use as a short–circuit excitation term for determining the aperture distribution. The technique has been found to be relatively simple to implement, and gives accurate results. Although only linear apertures with depth were investigated here, it should be possible to apply the method to more complex aperture configurations. It is noted that tortuous depth paths through the wall can be accounted for, in an approximate sense, by simply increasing the depth parameter in the equivalent radius; however, the effective depth must remain electrically small [10].

A potentially useful variation on the application of the HTSA is the following. Suppose that one desires to model a system that has high internal complexity, but low external complexity. If the exterior short–circuit field local to an aperture can be

approximated by analytic means, then the FDTD code with HTSA can be used to model only the interior region with only interior feedback. Because feedback is included in the interior, the resulting aperture field driving the cavity will be quite accurate, and therefore the predicted coupling to interior elements will also be quite accurate. This approach, of course, does not propagate the fields radiated by the aperture *into the exterior region*, but neglecting this will not significantly alter the interior response unless there exist external obstacles which would redirect this radiation back into the aperture; i.e., significantly alter the assumed external short–circuit fields to the extent that feedback would be required in the exterior region as well. Assuming that exterior feedback is *not* required, this type of approximation can result in considerable computer time and memory savings provided the exterior short–circuit field can be estimated. It is noted that as an exercise Test Problem 2 was solved *without* exterior feedback and the resulting waveforms differed only slightly from the those obtained *with* exterior feedback.

REFERENCES

[1] K.S. Yee,"Numerical solution of initial boundary value problems involving Maxwell's equations in isotropic media," *IEEE Trans. Ant. Prop.*, vol. AP–14, pp.302–307, May 1966.

[2] D.E. Merewether, "Transient currents induced on a body of revolution by an electromagnetic pulse," *IEEE Trans. EMC,* vol. EMC–13, 2, May 1971.

[3] A. Taflove, K.R. Umashankar, B.Beker, F. Harfoush, and K.S. Yee, "Detailed FD–TD analysis of electromagnetic fields penetrating narrow slots and lapped joints in thick conducting screens," *IEEE Trans. Ant. Prop.*, vol. AP–36, 2, pp. 247–257, Feb. 1988.

[4] J. Gilbert and R. Holland, "Implementation of the thin–slot formalism in the finite–difference EMP code THREDH," *IEEE Trans. Nucl. Sci.*, vol. NS–28, 6, pp.4269–4274, Dec. 1981.

[5] C.D. Turner and L.D. Bacon, "Evaluation of a thin–slot formalism for finite–difference time–domain electromagnetic codes," *IEEE Trans. EMC*, vol. 30, 4, pp. 523–528, Nov. 1988.

[6] A. Taflove and K. Umashankar, "A hybrid moment method/finite–difference time–domain approach to electromagnetic coupling and aperture penetration into complex geometries," *IEEE Trans. Ant. Prop.*, vol. AP–30, 4, pp. 617–627, July 1982.

[7] D.E. Merewether and R. Fisher, "Finite–difference analysis of EM fields inside complex cavities driven by large apertures," *IEEE Trans. EMC*, vol. EMC–24, 4, pp. 406–410, Nov. 1982.

[8] K.R. Demarest, "A finite–difference time–domain technique for modeling narrow apertures in conducting scatterers," *IEEE Trans. Ant. Prop.*, vol. AP–35, 7, pp. 826–831, July 1987.

[9] K.S. Yee and J.C. Kasher, "Modeling the electromagnetic coupling through small circumferential seams with FDTD," Lawrence Livermore National Lab. Tech. Report, UCRL–97239, Aug. 1987.

[10] L.K. Warne and K.C. Chen, "Equivalent antenna radius for narrow slot apertures having depth," *IEEE Trans. Ant. Prop.*, vol. AP–37, 7, pp. 824–834, July 1989.

[11] C.M. Butler and E.K. Reed, "Electromagnetic penetration through finite–length narrow slots in planar conducting screens," Lawrence Livermore National Lab./Clemson University Tech. Report, UCRL–21108, June 1988.

[12] A. Taflove and M.E. Brodwin, "Numerical solution of steady–state electromagnetic scattering problems using the time–dependent Maxwell's equations," *IEEE Trans. Microwave Theory Tech.*, vol. MTT–23, pp. 623–630, Aug. 1975.

[13] D.J. Riley and W.A. Davis, "Time–domain techniques in the singularity expansion method," AFWL Interaction Note 424, Air Force Weapons Laboratory, Albq. NM, Dec. 1982.

[14] D.J. Riley and W.A. Davis, "Application of an offset mesh for the transient, explicit finite–difference analysis of the perfectly conducting rectangular plate," *Radio Science*, vol. 20, 5, pp. 1031–1036, Sept.–Oct. 1985.

[15] L.K. Warne and K.C. Chen, "Slot apertures having depth and losses described by local transmission line theory," AFWL Interaction Note 467, Air Force Weapons Laboratory, Albq. NM, June 1988.

DISTRIBUTION:

Air Force Weapons Laboratory
Kirtland Air Force Base
Albuquerque, NM 87117–6008
Attn: R. J. Hamilton, AFWL/TALR (1)
D. A. Knight, AFWL/TALV (1)
M. Skinner, AFWL/TALE (1)
T. Cetticeri, AFWL/TAL (1)
B. Anderson, AFWL/AWPB (1)
S. Bigelow, AFWL/AWPB (1)
W. Baker, AFWL/AWP (1)
D. Voss, AFWL/AWPB (1)
P. Vail, AFWL/TAL (1)

Defense Nuclear Agency Headquarters
6801 Telegraph Rd.
Alexandria, VA 22310–3398
Attn: W. Goodell, Attn: SPLH (1)
P. Filios, Attn: RAEV (1)
G. Kwitkowski, Attn: RAEV (1)

EMA
5101 Copper Av. NE.
Albuquerque, NM 87110
Attn: D.E. Merewether (1)

General Dynamics–Pamona
401–01
P. O. Box 507
Pamona, CA 91769
Attn: R. McDonald (1)
K. Brown (1)

Harry Diamond Laboratory
2800 Powder Mill Rd.
Adelphi, MD 20783–1197
Attn: L. F. Libelo (1)
A. Bromborsky (1)
J. Tatum (1)

JAYCOR
11011 Torreyana Rd.
P. O. Box 85154
San Diego, CA 92121
Attn: E. P. Wenaas (1)
R. Leadon (1)

JAYCOR
39650 Liberty St.
Suite 320
Fremont, CA 94538
Attn: K. Casey (1)

Kaman Sciences/Dikewood Division
2800 – 28th St., Suite 370
Santa Monica, CA 90405
Attn: K.S.H. Lee (1)

Kaman Sciences
P. O. Box 7463
Colorado Springs, CO 80933
Attn: L. Allen (1)

Lawrence Livermore National Laboratory
University of California
P. O. Box 808
Livermore, CA 94550
Attn: R. J. King, L–156 (1)
S. L. Ray, L–156 (1)
H. Cabayan, L–86 (1)
R. Mcleod, L–156 (1)
S. Nelson, L–228 (1)
R. Zacharias, L–153 (1)

Los Alamos National Laboratory
University of California
P. O. Box 1663
Los Alamos, NM 87545
Attn: J. Toevs, MS–D408 (1)
J. Porter, MS–F617 (1)
B. Freeman, MS–J970 (1)
W. T. Armstrong, MS–D466 (1)
D. Bergan, MS–B218 (1)

Naval Research Laboratory
4555 Overlook Ave. SW
Washington, D. C. 20375–5000
Attn: A. W. Ali (1)
W. M. Manheimer (1)

Syracuse University
Department of Electrical and Computer Engineering
Syracuse, NY 13210
Attn: T. K. Sarkar (1)

Texas A&M University
Dept. of Electrical Engineering
College Station, TX 77843
Attn: R. D. Nevels (1)

U. S. Army Vulnerability Assessment Laboratory
White Sands Missile Range, NM 88002–5513
Attn: R. Flores (1)

Virginia Polytechnic Institute
Dept. of Electrical Engineering
Blacksburg, VA 24061
Attn: W. A. Davis (1)

Clemson University
Dept. of Electrical and Computer Engineering
Clemson SC 29634–0915
Attn: C. M. Butler (1)

Northwestern University
Technological Institute
Dept. of Electrical Engineering and Computer Science
Evanston, IL 60201
Attn: A. Taflove (1)

Lockheed Missiles and Space Co.
Sunnyvale, CA 94086
Attn: K. S. Yee (1)

EMA
P.O. Box 260263
Denver, CO 80226
Attn: J.E. Elliott

Computer Sciences Corporation – Systems Division
2100 Air Park Road, SE, Suite 200
Albuquerque, NM 87106
Attn: R.W. Holland

Mission Research Corporation
5434 Ruffin Road
San Diego, CA 92123
Attn: D.P. Snowden

University of Dundee
Department of Mathematical Sciences
DUNDEE DD1 4HN
Scotland, UK.
Attn: Paul D. Smith

University of Kansas
Department of Electrical and Computer Engineering
Lawrence, KS 66045
Attn: K.R. Demarest

1235 J. M. Hoffman
1235 J. F. Aurand
1235 L. D. Bacon
2311 J. D. Porter
2343 W.H. Schaedla
2343 B. C. Brock
3141 S. A. Landenberger (5)
3151 W. I. Klein (3)
3154–1 For DOE/OSTI (8)
7553 M. E. Morris
7553 L. K. Warne
7553 K. C. Chen
7554 L. D. Scott
7555 B. Boverie
8524 J. A. Wackerly
9300 J. E. Powell
9350 J. H. Renken
9351 E. F. Hartman
9352 G. J. Scrivner
9352 C. D. Turner (6)
9352 C. N. Vittitoe
9352 J. D. Kotulski
9352 D. J. Riley (20)

Org.	Bldg.	Name	Rec'd by	Org.	Bldg.	Name	Rec'd by
8524		Wackerly					
8524-2							

Sandia National Laboratories